SERPENTINE-NONTRONITE-VERMICULITE MIXED-LAYER CLAY FROM THE WECHES FORMATION, CLAIBORNE GROUP, MIDDLE EOCENE, NORTHEAST TEXAS

J. M. Huggett[1,*], D. K. McCarty[2], C. C. Calvert[3], A. S. Gale[4,5] and C. Kirk[1],

[1] Department of Mineralogy, The Natural History Museum, Cromwell Road, London SW7 5BD, UK
[2] ChevronTexaco, 3901 Briarpark, Houston, Texas, 77042, USA
[3] Department of Engineering Materials, University of Sheffield, Sheffield L1 3JD, UK
[4] Department of Earth & Environmental Sciences, The University of Greenwich, Chatham Maritime, Kent ME4 4TB, UK
[5] Department of Palaeontology, The Natural History Museum, Cromwell Road, London, SW7 5BD, UK

Abstract—The Weches Formation of the Claiborne Group (Eocene) in northeast Texas consists of clayey sandstones and mudrocks, both with variable proportions of dark green to brown clay peloids deposited in a marginal to open marine setting on the Gulf Coast margin. The composition of the dark green peloids, from two localities, has been investigated using X-ray diffraction, back-scattered electron microscopy with X-ray analysis, electron energy-loss spectroscopy (EELS), Mössbauer spectroscopy, chemical analysis and Fourier transform infrared spectroscopy. These peloids were previously described on the basis of their color as glauconite (Yancey and Davidoff, 1994); our results, however, show that the dark green indurated pellets are predominantly composed of mixed-layer clays with a high proportion of Fe-rich 7 Å serpentine layers coexisting with a mixed-layer phase containing glauconite, nontronite and vermiculite layers, in addition to discrete illite and kaolinte. Analyses by EELS of single particles with a chemical composition consistent with them being the Fe-rich clay indicate that the Fe is >95% ferric, while Mössbauer analyses of the bulk magnetically separated fraction for the same samples indicates a ferric iron content of ~$60-70\%$, despite the variable relative proportions of expandable and 7 Å layers. Taking into account that there is a significant amount of 2:1 layers containing ferric Fe, we interpret these data as indicating that the Fe in the 7 Å layers has a significant amount of Fe^{2+} even taking into account the high ferric Fe ratio from the EELS analysis when the coexisting 2:1 layers are considered. Thus, these 1:1 layers are closer to berthierine in composition than to odinite. The vermiculite layers in the Texas clay may indicate partial 'verdinization' of expandable 2:1 clay. A possible reaction is smectite → vermiculite → berthierine-like phase. We estimate a temperature of 20ºC for the seawater in which the Texas clay formed, the lower end of the range for modern occurrences of odinite.

Key Words—Clay Pellets, EELS, Mössbauer Spectroscopy, Serpentine-nontronite-vermiculite, Verdinization, Texas, Weches Formation.

INTRODUCTION

The objective of this study was to determine the composition and origin of the green clay pellets in the Claiborne Group. The green granule-forming clays are mixed-layer assemblages containing layers of glauconite, nontronite, and a 7 Å serpentine group component that we interpret as berthierine-like (McCarty *et al.*, 2004), which occurs as the dominant layer in mixed-layer phases with glauconite and nontronite layers. Glauconite is a green, ferric Fe-rich micaceous mineral that forms in marine sediments, often associated with and replacing nontronite. Odinite and ferric chlorite are the ferric Fe-rich precursors of the ferrous Fe-rich clays berthierine and chamosite. Fe-rich authigenic ~7 Å and ~14 Å non-expanding and weakly expanding clay minerals in recent sediments were identified as phyllite V and phyllite C by Odin (1988), who named the clay facies that they dominate 'verdine facies'. Phyllite C is a ferric chlorite with a minor swelling component, while phyllite V encompasses the clay now known as odinite, though its characteristics are more variable than those of odinite. Odinite is only known from recent marine sediments. Iron-rich authigenic 7 Å and 14 Å clays identified in ancient marine and non-marine sediments occur mostly as ooidal coatings (*e.g.* Bhattacharyya, 1983; Chamley, 1989, and references therein; Macquaker *et al.*, 1996; Taylor, 1998) or grain-rimming clay (*e.g.* Imam and Shaw, 1985), though this may in part be a consequence of a tendency amongst field geologists to describe pelloidal green clay as glauconite and ooidal clays as 'chlorite'. The Fe-rich 7 Å clay in sediments <15,000 years old is odinite, a clay associated with fecal peloids found exclusively in the tropics (mainly between 16ºN and 23ºS), where the water temperature is >20ºC (Porrenga, 1967; Van Houten and Purucker, 1984; Odin, 1988; Odin *et al.*, 1988a, 1988b; Odin and Sen Gupta, 1988). The only ancient odinite known to us occurs in the Miocene sediments cored in the Niger Delta (Porrenga, 1965; Odin *et al.*, 1988a). On the basis of our findings for the Claiborne Group green

* E-mail address of corresponding author:
JMHuggett@petroclays.demon.co.uk

clay pellets, we suggest that a more detailed analysis might show that this odinite is also a mixed-layer clay.

Berthierine is rich in ferrous Fe (typically $29-37$ wt.%) with a small percentage of ferric Fe (typically $0.2-5.5\%$); the octahedral sheet also contains MgO (typically $2-5$ wt.%) and Al_2O_3 (typically $20-25$ wt.%) (Brindley, 1982). Odinite is ferric Fe-rich, with an FeIII:FeII ratio usually <3, and contains more MgO than berthierine (Bailey, 1988). Berthierine is not known from recent sediments and it is tentatively but widely assumed that it is formed from odinite by diagenetic Fe reduction and loss of MgO (*e.g.* Ryan and Hillier, 2002). However, ancient berthierine is found in a wide range of environments, including high-latitude and non-marine sediments (Shterenberg *et al.*, 1968; Taylor, 1990).

GEOLOGICAL SETTING

The Claiborne Group (Lutetian age—middle Eocene) in Texas contains clay-rich sandstone and mudstone units deposited in marginal marine shelf and estuarine environments (Yancy and Davidoff, 1994). Sediments prograded across a narrow shelf, during a period of overall sea-level rise (Vincent and Ewing, 2000). Previous work by Burst (1958) and Wermund (1961) has shown the presence of both "glauconite" and "chloritic clay" (their term for the 7 Å Fe-rich clay) as

replacement of fecal peloids and fossil test infilling, in the Claiborne Group. Clay peloids which are composed completely, or nearly so, of Fe-rich 7 Å clay are typically lithified and dark olive or emerald green. Brown peloids composed mainly of Fe smectite are also present but are not discussed here.

Samples were obtained from the Weches Formation at Nacogdoches and Hooker Creek (Figure 1). The Weches Formation is exposed (13.5 m) between the margin of Lake Nacogdoches and Texas Highway 225, Nacogdoches County. A single nanoplankton date (data kindly provided by M.-P. Aubry) indicates that the top of the Nacogdoches section falls within NP15b, which is ~45 Ma (mid-Lutetian). The entire section is part of a transgressive systems tract deposited in a shallow shelf setting. The fauna and frequent bioturbation indicate deposition in an oxic marine environment, while the high proportion of clay in the sediment indicates a low-energy environment. This interval of the Weches Formation contains a greater proportion of Fe-rich clay peloids ($\leqslant 45\%$ point-counted) than is found in the other Claiborne Group exposures sampled ($\leqslant 30\%$). Four samples have been analyzed from Nacogdoches, though one (NAC6) was collected from the same bed as NREK1 because the latter sample proved too small for all the analyses to be performed. Hooker Creek (two samples analyzed) is located near Liberty Church, off Texas Highway 908, 7 km west of Caldwell, Burleson County.
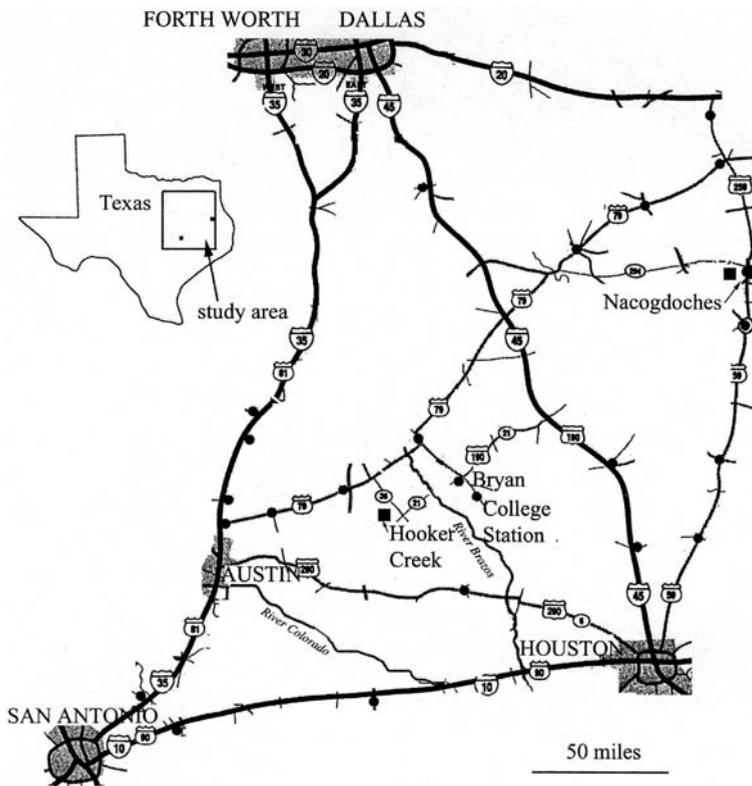

Figure 1. Map of NE Texas showing the approximate location of the two sampled localities.

At the time of our visit 2.55 m of mudrock of the Weches Formation were exposed in the stream. The abundant, predominantly molluscan fauna is marine and has been described by Zachos (1993). Most of the section is sandy silty mudstone with 20−50% green peloids. The peloids and sand grains are concentrated in burrows and horizontal lenses.

METHODOLOGY

Six samples (four from Nacogdoches, two from Hooker Creek) with peloids particularly rich in green, Fe-rich clay were selected from a much larger sample suite which had been subjected to extensive whole-rock mineralogical, paleontological and sedimentological analysis (to be reported elsewhere). The peloids, which are sand-sized particles, were separated from the matrix by sieving to extract the >63 μm fraction followed by magnetic separation of the Fe-rich peloids from the non-magnetic fraction (note that this method does not separate the clay or silt-grade quartz within peloids from the Fe-rich clay). The sieved samples were placed in an ultrasonic bath to break up any of the softer brown, Fe smectite-rich peloids and disperse the matrix. The suspension was poured off and the remaining green clay peloids washed to remove all traces of dispersed clay. Splits of these samples were used for X-ray diffraction (XRD), EELS and Mössbauer analysis.

A portion of each separate was ground with ~5 mL of water in a rod mill for just 1 min to break the peloids into a clay slurry. Analysis by XRD of the clay fraction of the crushed peloids (<4 μm) was carried out using a Philips 1820 automated X-ray diffractometer with CuKα radiation. Dried, oriented mounts on unglazed tiles were scanned at a rate of 5 s per 0.02°2θ step, using 0.3 mm slits from 2 to 40°2θ. After spraying with ethylene glycol, they were rescanned from 2 to 26°2θ and again after heating at 400°C for 4 h, and after heating at 550°C, also for 4 h. A further portion of sample was treated with 50% HCl for 30 min at 100°C, washed three times and then prepared as above for clay-fraction XRD. The hot acid dissolves Fe-rich 7 Å and 14 Å clay, hence an absence or drop in 7 Å (and higher order) reflection intensity after acid treatment indicates the presence of Fe-rich 7 Å clay in the untreated sample. The d values were calibrated against the quartz reflection at 4.259 Å. The results of these analyses were used to select samples for more detailed XRD analysis and pattern simulation.

For the purpose of crystallographic indexing, ~20 of the peloids of sample NREK1 were hand-picked under a binocular microscope, ground, packed into a random powder mount and analyzed using a Nonius Diffractometer in reflection geometry with CuKα[1] radiation, Ge monochromator and an INEL position-sensitive detector. Data were collected for 2 h.

Full-pattern computer simulation is probably the most effective way to reveal the structural details of complex mixtures (e.g. Drits et al., 1997, 2002; Sakharov et al., 1999; Plançon, 2004). The multispecimen fitting technique simulates diffraction data from the scans of both the ethylene glycol-treated and air-dried sample. The particular method we have used is the computer program of Drits and Sakharov (unpublished); the mathematical formalisms may be found in Drits and Tchoubar (1990). The result is judged to be reasonable when the best fit is obtained for both of these simulations using the same structural parameters. The advantages of this approach to simulation of mixed-layer clays, compared with the traditional Markovian model, were discussed fully by Plançon (2004).

For the purpose of computer modeling, selected samples were re-analyzed by XRD in the ChevronTexaco XRD Laboratory in Houston. The methodology for these analyses was as follows. The <2.0 μm equivalent spherical diameter size fraction was separated from samples by standard centrifugation methods. The samples selected for detailed study were treated to remove carbonate and Fe-Fe oxide cements with Na-acetate buffer and Na dithionite, respectively (Jackson, 1985). The Na^+-saturated clays were exchanged with Ca^{2+} using Ca cation-exchange resin beads. Approximately 250 mL of <2.0 μm suspension were shaken overnight with ~5 g of Dowex® HCR-W2 resin beads. The suspension was then dried and oriented aggregates were made by evaporation onto glass slides to provide a sample ~4 cm long with at least 10 mg of clay per cm^2 (Moore and Reynolds, 1997). Diffraction scans for each sample were collected with a Scintag X1 diffractometer equipped with a solid-state Si detector, after ethylene glycol (EG) treatment by vapor solvation in a heated chamber and also in the ambient (air-dried) state. The scans were made from 2 to 52°2θ with a 0.02°2θ step increment and counting rate of 4 s per step or longer using CuKα radiation transmitted through a 2.0 mm divergence and 4 mm scatter slit. Detector slits were 0.5 mm and 0.2 mm. Samples selected for pattern simulations were the 7 Å clay-rich samples NREK6, NREK7, NAC6 and HCW1.

Carbon-coated, polished thin-sections of all samples were examined using back-scattered electron imaging (BSEI) in a Jeol 3510LV scanning electron microscope (SEM) with an Oxford Instruments detector (Be window) and ISIS microanalysis software. Quantitative energy dispersive X-ray (EDS) analyses were obtained from polished blocks using a 2 μA beam current at 15 kV accelerating voltage.

Electron energy-loss spectroscopy is a transmission electron microscopy (TEM) technique that permits determination of Fe^{3+} and Fe^{2+} in single-mineral particles. This avoids inclusion of other Fe-bearing minerals in the analyses. The methodology is described by Calvert et al. (2004). The equipment used was an FEI CM200 FEGTEM operated at 200 keV fitted with a Gatan imaging filter (GIF) and an Oxford Instruments

UTW (ultra thin window) ISIS EDX system. Five samples of <2 μm fraction clay were prepared by dispersion onto TEM grids (400 μm mesh copper grids with a holey carbon film support). For each area analyzed, an EDX spectrum was collected first and then the EELS spectrum. All EELS measurements were made in CTEM diffraction mode (image coupling to spectrometer) on ultrathin (<30 nm) crystalline areas of dimension ~0.1 μm. All spectra were corrected for dark count and detector gain. Ultrathin areas were chosen to avoid the need for deconvolution. For each sample, six Fe $L_{2,3}$-, O K-edges and their associated low-energy loss spectra were collected, with total integration times of 20−30 s for Fe $L_{2,3}$-edges and 10−20 s for O K-edges at an energy dispersion of 0.1 eV/pixel (analysis times

>30 s result in progressive reduction of Fe^{3+} to Fe^{2+}). The 0.6 mm EELS entrance aperture was used to give a collection angle of 4.6 mrads. The energy resolution of the zero-loss (low loss) peak for all measurements was 0.7−0.8 eV. The EELS data were collected from six areas of each sample. A representative example of the Fe $L_{2,3}$- and O K edges is shown for each sample. Prior to EELS analysis, EDS spectra were collected to confirm that the particle selected was Fe-rich and contained <0.5% of Ca, K or Na.

Mössbauer spectra were obtained for four samples (those for which we carried out XRD pattern simulation) using a constant acceleration spectrometer and a source of ^{57}Co in Pd. Isomer shifts are given relative to the centroid of the spectrum of the α-Fe at room tempera-
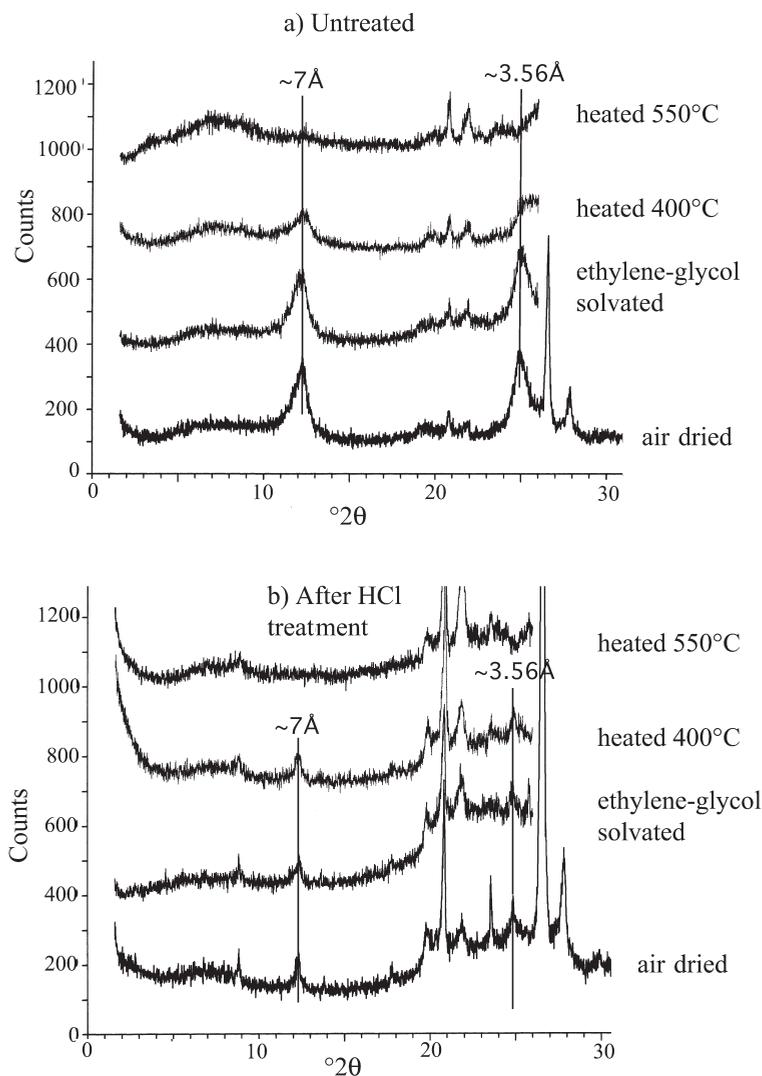
Figure 2. XRD traces of oriented clay from magnetically separated green clay peloids from NREK1. The broad band of low intensity at ~5º2θ on the untreated sample may be due to a small amount of swelling clay. The enhanced low-angle intensity at ~5º2θ on the heated and acid-treated samples is inferred to be at least in part due to degradation products of odinite. The 7 Å reflections on the acid-treated samples are due to kaolinite.

ture. The analysis was performed on Na-saturated <2 μm clay separations at room temperature and with absorbed plane at an angle of 54.7° to the radiation. Lorentzian line shape was used to determine ferrous and ferric octahedral cations ratios.

For chemical analysis of the Fe^{2+} content, powdered samples of <2 μm fraction clay were digested in HF/H_2SO_4 and the oxidizable species titrated against $KMnO_4$.

Fourier transform infrared (FTIR) analysis was carried out on the same samples as used for XRD pattern simulation. As with clay separation for XRD, samples for FTIR analysis were treated using the buffered Na acetate and Na dithionite methods of Jackson (1985). The <2 μm size fraction was obtained by centrifugation and dried in an oven at ~80°C. Approximately 100 mg of this dried sample were then prepared and analyzed as described by McCarty *et al.* (2004). The purpose of these analyses was to determine whether kaolinite could be detected in the samples prior to XRD pattern simulation. The FTIR and XRD pattern simulation work was carried out at ChevronTexaco.

RESULTS

XRD data

The preliminary XRD data for the peloids show broad clay reflections, indicative of small crystallite size or abundant crystal defects. Sharp reflections at 3.34 Å and in some samples at 4.249 Å, indicate the presence of small amounts of quartz, while a sharp reflection at 3.19 Å indicates feldspar in the <4 μm fraction of NREK1 (Figure 2) and HCW1. All the samples selected for this study have large number of of 7 Å layers, along with glauconite and nontronite layers, plus discrete kaolinite and illite. NREK1 is apparently pure 7 Å. Distinguishing between poorly crystalline kaolinite and poorly crystalline Fe-rich 7 Å clay is not easy, as, unlike chlorite and $1M$ berthierine, the 002 reflection of Fe-rich 7 Å serpentine overlaps that of kaolinite, at 3.56 Å (Figure 2). The loss of intensity after heating at 400°C is characteristic of Fe-rich 7 Å clay, but this alone is insufficient for identification. The hot HCl test described above results in significant loss of 7 Å reflection intensity after the treatment (Figure 2b), confirming that Fe-rich 7 Å serpentine is the predominant clay with little or no kaolinite present (Figure 2). The enhanced low-angle intensity at 5−7°2θ on the heated and acid-treated samples is inferred to be at least in part due to degradation products of the 7 Å layers.

Measurement of the clay 060 reflections on powdered samples also proved difficult due to the breadth of reflections caused by the disordered structure and overlap with odinite $\bar{3}31$ and berthierine $33\bar{4}$ reflections. However, the calculated reflection position of 1.5437 Å (after quartz subtraction) is consistent with an Fe-rich 7 Å serpentine composition. In most samples the

kaolinite reflection at 1.488 Å was also detected. No kaolinite was detected in sample NREK1 by the preliminary XRD and this sample was therefore the one selected for powder diffraction and used for indexing (Figure 3). Due to the poor crystallinity of the mineral the reflections are broad and weak; hence the calculated cell parameters are only approximate. Two reflections (002 and 040) could be indexed singly (*i.e.* without interference from other reflections), while a further two ($\bar{3}31$ and 330) were indexed after decomposition; these reflections are listed in Table 1. The approximate unit-cell parameters (±0.05 Å) for a C-centered monoclinic cell are: a = 5.34 Å, b = 9.29 Å, c = 7.33 Å and β = 103.7°. These parameters differ from those calculated by Bailey (1988) for the $1M$ odinite from recent sediments by only ~0.03 Å for the spacings and 0.3° for the β value. The observed reflections used for indexing differ by ~0.01 Å from Bailey's values for $1M$ odinite (Table 1). However, because of the uncertainties about the true peak position due to the disordered serpentine layer structure, the exact species cannot be determined from the random powder data alone.

EELS analysis

For EELS analysis we were careful to analyze only clay particles with a composition dominated by 7 Å layers to determine if these layers are berthierine or odinite-like. Samples HCW1 and NREK6 were very easily damaged by the electron beam and have EDS spectra (those collected from single particles during TEM analysis) that show small amounts of K; this is consistent with a small amount of illite or mica contamination of the 7 Å mineral (Figure 4). Samples NREK1 (Figure 4) and NREK4 have EDS spectra with no more than trace K. Sodium and Ca were not detected in any particle selected for EELS, indicating an absence of detectable smectite contamination.
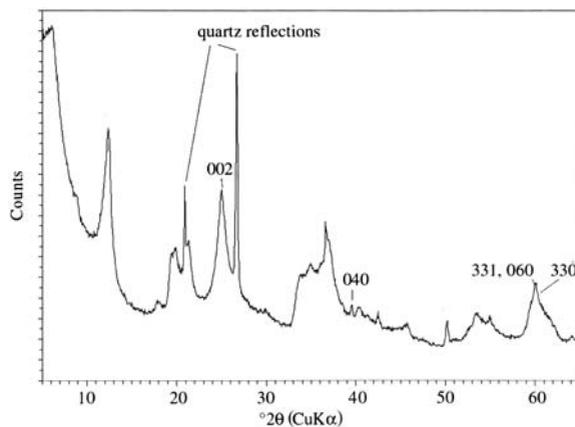

Figure 3. Powder diffraction trace of magnetically separated green clay peloids from NREK6. The reflections marked are those used for indexing. Quartz reflections are also marked. Note the absence of Fe oxide or hydroxide reflections.

Table 1. Reflection positions, relative intensities and *hkl* data for 1*M* berthierine (data from Brindley, 1951), for berthierine 1*H* (data from Brindley and Youell, 1953), odinite (data from Bailey, 1988) and NREK1. The NREK1 data in bold type are those used for indexing.

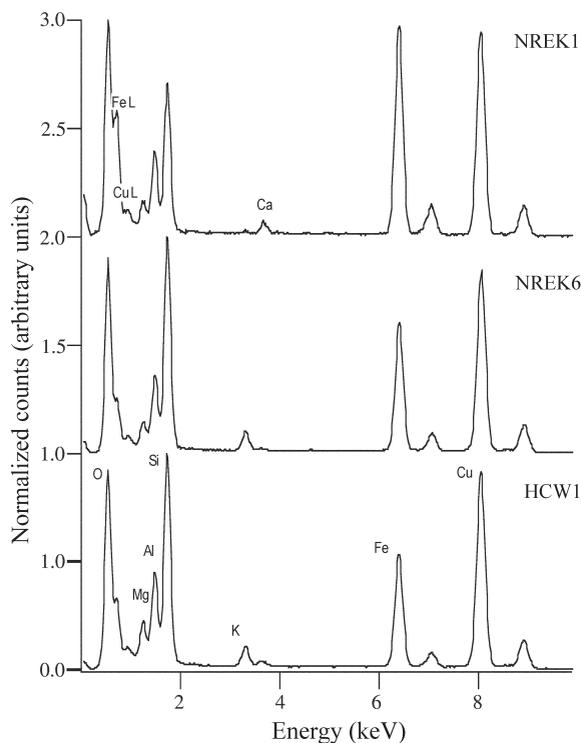| Berthierine-1*M*			Berthierine-1*H*			Odinite-1*M*			NREK1		
d (meas.)	Intensity	*hkl*	*d* (meas.)	Intensity	*hkl*	*d* (meas.)	Intensity	*hkl*	*d* (meas.)	Intensity	*hkl*
7.050	100	0 0 1	7.12	100	0 0 1	7.15	100	0 0 1	7.270		
4.670	20	0 2 0	4.68	50	1 0 0	4.65	40	0 2 0			
4.580	20	1 1 0	4.3	20		4.53	20	$\bar{1}$ 1 0	4.560		
4.280	5	$\bar{1}$ 1 1	3.93	30	1 0 1	3.58	85	0 0 2	**3.564**	**40**	**0 0 2**
3.900	10	0 2 1	3.55	100	0 0 2	2.84	1	0 2 2	2.785		
3.520	100	0 0 2	3.07	20		2.67	40	1 3 0/2 0 $\bar{1}$	2.596		
2.800	1	0 2 2	2.71	50	1 1 0	2.56	7	1 1 2			
2.68	40	$\bar{2}$ 0 1	2.53	100	1 1 1	2.51	3				
2.52	90	1 1 2	2.15	70	1 1 2	2.41	30	1 3 1/2 0 $\bar{2}$	2.329	**60**	**0 4 0**
2.400	40	1 3 1	1.77	60	0 0 4	2.34	5	0 4 0	2.287		
2.340	5	0 4 0	1.563	70	3 0 0	2.15	1	$\bar{2}$ 2 2	2.202		
2.270	5	$\bar{1}$ 3 2	1.526	50	3 0 1	2.02	10	1 3 2/2 0 $\bar{3}$	2.013		
2.140	60	$\bar{2}$ 2 2	1.481	60	1 1 4	1.9	2	2 0 2/1 3 $\bar{3}$	1.630		
2.010	10	1 3 2	1.433	40	3 0 2	1.74	7	2 4 0			
1.890	10	$\bar{1}$ 3 3	1.416	10	2 0 4	1.67	7	1 3 3/2 0 $\bar{4}$			
1.760	40	$\bar{3}$ 1 1	1.327	40	2 2 1	1.62	2	1 5 $\bar{2}$/2 4 1			
1.700	1					1.552	65	$\bar{3}$ 3 1	**1.544**	**79**	**$\bar{3}$ 3 1**
1.665	5	1 3 3				1.517	10	3 3 0	**1.511**	**76**	**3 3 0**
1.555	70	0 6 0				1.49	3	2 2 3	1.437		
1.520	30	3 3 0				1.43	5	0 6 2/3 3 1	1.357		
1.473	10	$\bar{1}$ 5 3				1.33	15	$\bar{1}$ 3 5/2 0 4	1.321		
1.425	10	3 3 1							1.290		
1.407	5	0 4 4							1.245		
1.361	5	$\bar{2}$ 4 4							1.021		
1.347	5	$\bar{2}$ 6 1									
1.326	5										

Figure 4. EDS spectra collected from single clay particles during TEM analysis.

The Fe $L_{2,3}$ edges which show a peak maximum at 709.5eV energy loss are indicative of Fe^{3+}, while the Fe $L_{2,3}$ edges which show a peak maximum at 707.5eV energy loss are indicative of Fe^{2+}. The Fe $L_{2,3}$ edges peak maxima for all five samples occur at 709.5 eV energy loss, with a shoulder at ~707.5 eV (Figure 5). Fe^{2+} was not detected in any of the samples, though as the fitting program (Calvert *et al.*, 2001, 2004) has a detection limit of 5% Fe^2, <5% Fe^{2+} may be present. These data suggest that the $Fe^{3+}/(Fe^{2+}+Fe^{3+})$ in the Fe-rich and Ca-, K-, Na- poor clay is >0.95 (0.95 is the detection limit for $Fe^{3+}/(Fe^{2+}+Fe^{3+})$). The O-K edges show a pre-peak at ~531 eV, a well defined peak at ~540 eV and a broad peak at ~565 eV (Figure 5). The pre-peak at ~531 eV suggests that the Fe is Fe^{3+}, producing strong hybridization of the O $1sp2$ and Fe $3d$ bonds. Both the Fe L2,3 and O K edges suggest that Fe is in octahedral co-ordination with O. These data match those collected from chlorite containing >.95 Fe as Fe^{3+} and not those of Fe oxides and hydroxides (Calvert *et al.*, 2004).

Mössbauer analysis

The data (Table 2, Figure 6) suggest a smaller proportion of Fe^{3+} in magnetically separated pellets as a whole than was determined by EELS analysis of single selected particles. The Mössbauer analysis was carried
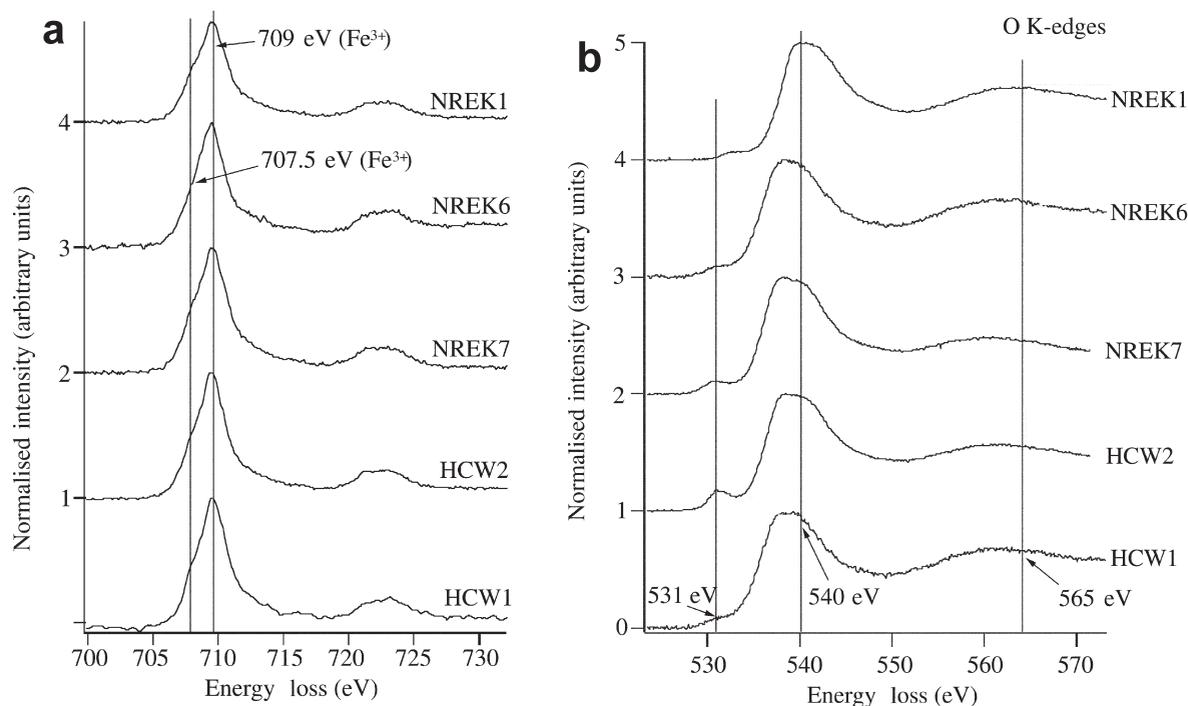
Figure 5. (a) EELS FeL2,3 edge data for NREK1, NREK6, NREK7, HCW2 and HCW1. FeL2,3 edges peak maxima occur at 709.5 eV energy loss with a shoulder at 708 eV for all samples. (b) EELS O-K edge data for NREK1, NREK6, NREK7, HCW2 and HCW1. These data match those collected from chlorite containing all Fe as Fe^{3+}; the pre-peak shoulder at ~533 eV indicates that the Fe is Fe^{3+} and in octahedral co-ordination.

out on a split of the <2 μm material that was used in the XRD analysis of the oriented sample and computer simulation; thus the $Fe^{3+}/(Fe^{2+}+Fe^{3+})$ ratio reflects the average value of all the different clay and other phases present. The chemical titration data for NREK 6, NREK7 and HCW1 give $Fe^{3+}/(Fe^{2+}+Fe^{3+})$ ratios closer to those obtained by EELS than those obtained by Mössbauer analysis (Table 3).

XRD pattern simulation

The structural models for illite-smectite diffraction calculations are as described by Sakharov *et al.* (1999). The *Z* co-ordinates and site occupancies, including those for one and two-layer glycol complexes, are taken from Moore and Reynolds (1997). The most significant diffraction effect from site occupancy is the content of octahedral Fe and this is not as significant or robust as

the proportion of layers and their junction probabilities. Other individual simulation parameters such as orientation effects, CSD, distribution of fundamental particles, proportion of layers and their junction probabilities all affect different regions of the diffraction pattern in different ways. This is the important aspect of the multispecimen profile-fitting method (*e.g.* Sakharov *et al.*, 1999 and citations therein). It is the combination of these parameters that allows a good fit of the entire diffraction profile. In the process of fitting, if an adjustment of one parameter results in a better fit in one portion of the profile, but causes a mis-fit in another portion, then it is rejected. The test for an acceptable model is a good fit in both the air-dried and ethylene glycol states with corresponding parameters (Table 3). We define smectite and vermiculite, or high-charged smectite, layers as those that swell to 16.6–16.9 Å and to 12.9–13.5 Å, respectively, when solvated with ethylene glycol (*e.g.* McCarty *et al.*, 2004; Drits *et. al.*, 2002). Even though pure Ca-vermiculite saturated with ethylene glycol may have a basal spacing of ~16 Å (MacEwan and Wilson, 1980) the basal spacings of high-charged layers in the I-S in this study are significantly smaller. To simulate the broad reflection at ~7 Å required a randomly interstratified (R0) Fe-rich 7 Å-nontronite-vermiculite composition. At this stage it was not possible to determine whether the Fe-rich clay was berthierine or odinite. This was done by considering

Table 2. Mössbauer and titration data. Numbers in parentheses are those obtained by titration.

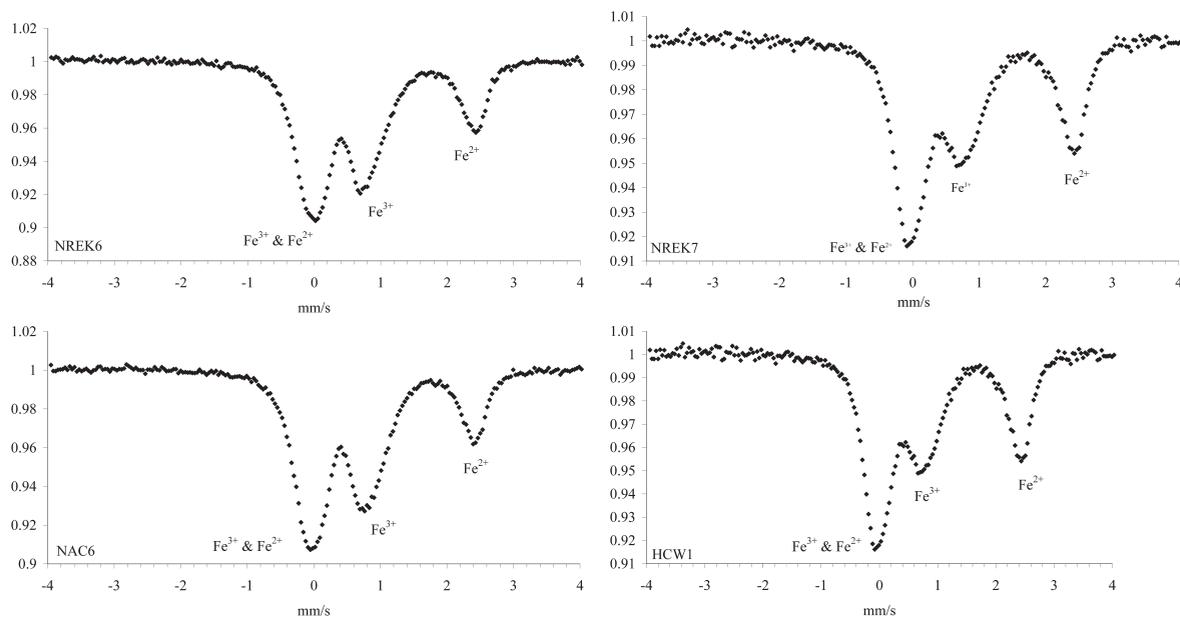|	% Fe^{2+}	% Fe^{3+}
NREK 6	30 (7.24)	70 (92.76)
NREK 7	31	69
NAC6	27	73
HCW1	42 (8.10)	58 (91.90)

Figure 6. Mössbauer spectra for NREK6, NREK7, NAC6 and HCW1.

the bulk chemistry and the EELS and Mössbauer analysis (see above). The proportions of the interlayers are shown in Figure 7 and Table 3. NAC6 required two different compositions of randomly interstratified serpentine-nontronite-vermiculite (R0 Sp-N-V). The other three samples that were modeled contain mixed-layer glauconite-nontronite-vermiculite (G-N-V) and all four contain minor amounts of kaolinite and illite (Figure 7). In the case of HCW1, the air-dried simulation additionally required a four component mixed-layer structure with two vermiculitic layers indicating more layer-charge heterogeneity (Table 3).

Analysis by FTIR confirmed the presence of kaolinite in all four samples (one of which, NREK7, is shown in Figure 8) and this information was used to improve the accuracy of the simulation. Quartz is also present (BSEM images confirm the presence of silt-grade particles within peloids) but has not been included in the simulation. The mis-fit of the simulated patterns $\sim20°2\theta$ and $33-38°2\theta$ is due to disorder, disorientation and contamination from non-clay.

Chemical composition

The analyses in Table 4 are not representative of the Weches Formation as a whole, but are the closest we could get to the pure Fe-rich 7 Å clay in the green clay peloids. The data in Table 4 were obtained from average point-specific SEM/EDS analyses, where the EDS points were chosen to avoid non-clays. Weight % K_2O and Na_2O were used as purity indicators (for illite and nontronite-vermiculite contamination, respectively). No analyses were obtained without trace amounts of these elements. In order to obtain an approximation of the mixed-layer clay composition, analyses with >2.5 wt.% of K and >0.25 wt.% of Na were omitted. Very small amounts of P_2O_5 ($\leqslant0.19$ wt.%) detected are due to apatite inclusions in the peloids. These and an appropriate proportion of CaO have been subtracted from the analyses (Table 4). The data have been normalized to facilitate comparison with the published data.

If the oxide chemistry for NREK6 is assumed to be only from the serpentine layers and the ferric:ferrous Fe ratio is as found by Mössbauer, then FeO = 12.21% and Fe_2O_3 = 33.03%. This means the average structural formula for the hypothetical serpentine layer is:

$$(Si_{3.19}Al_{0.81})(Al_{0.69}Fe^{3+}_{2.34}Fe^{2+}_{0.96}Mg_{0.90})O_{10}(OH)_8$$
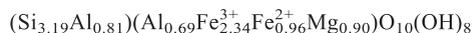
This formula is much closer to a berthierine composition than to odinite as ferrous Fe is too high for the sample to be odinite. Moreover, if any amounts of glauconite or nontronite layers are taken into account, then some Fe^{3+} must be assigned to such layers thereby increasing the Fe^{2+} content in the serpentine layer structural formula thus making it even closer to berthierine.

If the oxide chemistry (EDS X-ray analyses) for NREK6 is assumed to be from only the serpentine layers and the ferric:ferrous Fe ratio is as found by EELS, then FeO = 2.25% and Fe_2O_3 = 42.74% and the average serpentine layer formula is:

$$(Si_{3.13}Al_{0.87})(Al_{0.60}Fe^{3+}_{2.98}Fe^{2+}_{0.17}Mg_{0.88})O_{10}(OH)_8$$
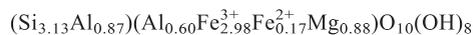
This formula is close to odinite. However, if any amounts of glauconite or nontronite layers are taken into account (they are known to be present in the sample) (Figure 7; Table 3), then a significant amount of the

Table 3. Weight concentration (%) of coexisting discrete and mixed-layer phases, as well as layer types, their thicknesses and contents determined by XRD simulations are given for specimens of each sample in air-dried and ethylene solvated states, g = glauconite, n = nontronite, v_1 = high-charge vermiculite, v_2 = low-charge vermiculite layer, Pgg = probability of a glauconite layer following a glauconite layer, and so on for other layer combinations.

Sample	EG, NREK6	Air-dried, NREK6	EG, NREK7
% g-n-v_1 in sample	R1 g-n-v_1 = 34%	R1 g-n-v_1 = 30%	R1 g-n-v_1 = 28%
d spacings	9.98 Å, 16.6 Å, 13.9 Å	9.98 Å, 14.9 Å, 12.4 Å	10.01 Å, 16.7 Å, 13.6 Å
proportions of each layer type	0.47 - 0.48 - 0.07	0.49 - 0.46 - 0.05	0.63 - 0.30 - 0.06
Probabilities for layer combinations (see caption for mineral codes)	Pgg = 0.56 Pgn = 0.28 Pgv$_1$ = 0.16 Png = 0.43 Pmm = 0.57 Pnv$_1$ = 0 Pv$_1$g = 0.17 Pv$_1$n = 0.83 Pv$_1$v$_1$ = 0	Pgg = 0.59 Pgn = 0.30 Pgv$_1$ = 0.10 Png = 0.36 Pmm = 0.63 Pnv$_1$ = 0 Pv$_1$g = 0.63 Pv$_1$n = 0.36 Pv$_1$v$_1$ = 0	Pgg = 0.70 Pgn = 0.29 Pgv$_1$ = 0.0 Png = 0.56 Pmm = 0.55 Pnv$_1$ = 0 Pv$_1$g = 0.27 Pv$_1$n = 0.72 Pv$_1$v$_1$ = 0
% Sp-n-v_1 in sample	R0 Sp-n-v_1 = 52%	R0 Sp-n-v_1 = 58%	R0 Sp-n-v_1 = 60%
d spacings	7.22 Å, 16.84 Å, 12.9 Å	7.13 Å, 15.1 Å, 12.5 Å	7.22 Å, 16.84 Å, 12.9 Å
proportions of each layer type	0.80 - 0.12 - 0.08	0.80 - 0.12 - 0.08	0.80 - 0.08 - 0.12
% illite in sample	Illite = 11%	Illite = 10%	Illite = 9%
% kaolinite in sample	Kaolinite = 3%	Kaolinite = 4%	Kaolinite = 3%

Sample	Air-dried, NREK7	EG, HCW1	Air-dried, HCW1
% g-n-v_1 in sample	R1 g-n-v_1 = 26%	R1 g-n-v_1 = 54%	R1-g-n-v_1-v_2 = 52%
d spacings	10.01 Å, 14.9 Å, 12.7 Å	9.98 Å, 17.05 Å, 13.0 Å	9.98 Å, 14.8 Å, 12.5 Å, 14.0 Å
proportions of each layer type	0.60 - 0.25 - 0.15	0.55 - 0.29 - 0.16	0.62 - 0.21 - 0.07 - 0.10
Probabilities for layer combinations (see caption for mineral codes)	Pgg = 0.70 Pgn = 0.15 Pgv$_1$ = 0.15 Png = 0.43 Pmm = 0.31 Pnv$_1$ = 0.24 Pv$_1$g = 0.47 Pv$_1$n = 0.52 Pv$_1$v$_1$ = 0	Pgg = 0.53 Pgn = 0.35 Pgv$_1$ = 0.12 Png = 0.44 Pmm = P0.28 Pnv$_1$ = 0.28 Pv$_1$g = 0.84 Pv$_1$n = 0.07 Pv$_1$v$_1$ = 0.09	Pgg = 0.72 Pgn = 0.15 Pgv$_1$ = 0.04 Png = 0.23 Pmm = 0.36 Pgv$_2$ = 0.09 Pnv$_1$ = 0.21 Pv$_1$g = 0.50 Pv$_1$n = 0.38 Pv$_1$v$_1$ = 0.09 Pnv$_2$ = 0.21
% Sp-n-v_1 in sample	R0 Sp-n-v_1 = 61%	R0 Sp-n-v_1 = 35%	R0 Sp-n-v_1 = 36%
d spacings	7.13 Å, 15.1 Å, 12.5 Å	7.19 Å, 16.9 Å, 13.8 Å	7.17 Å, 14.8 Å, 12.8 Å
proportions of each layer type	0.86 - 0.05 - 0.09	0.80 - 0.10 - 0.10	0.80 - 0.10 - 0.10
% illite in sample	Illite = 10%	Illite = 7%	Illite = 6%
% kaolinite in sample>	Kaolinite = 3%	Kaolinite = 4%	Kaolinite = 5%

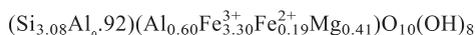| Sample	EG, NAC6	Air-dried, NAC6
% g-n-v_1 in sample	R0 g-n-v_1 = 69%	R0 g-n-v_1 = 66%
d spacings	7.05 Å, 16.5 Å, 13.8 Å	7.12 Å, 14.8 Å, 12.8 Å
proportions of each layer type	0.20 - 0.66 - 0.14	0.23 - 0.70 - 0.07
Probabilities for layer combinations (see caption for mineral codes)		
% Sp-n-v_1 in sample	R0 g-n-v_1 = 20%	R0 g-n-v_1 = 20%
d spacings	7.22 Å, 17.2 Å, 12.9 Å	7.15 Å, 15.0 Å, 12.8 Å
proportions of each layer type	0.75 - 0.18 - 0.7	0.75 - 0.13 - 0.12
% illite in sample	Illite = 3%	Illite = 6%
% kaolinite in sample	Kaolinite = 9%	Kaolinite = 8%
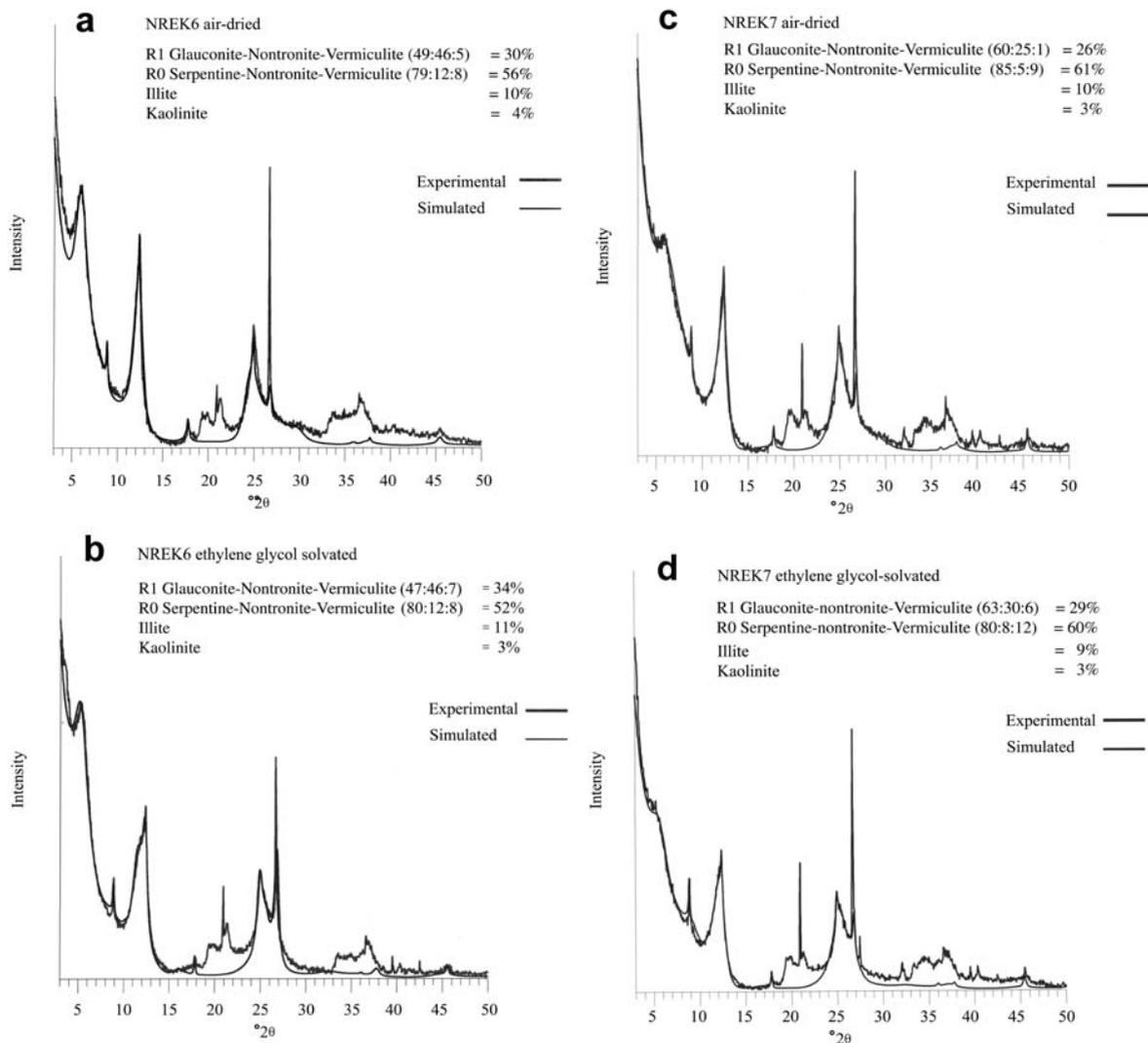
Figure 7 (*above and facing page*). XRD pattern simulations.

ferric Fe must be assigned to these layers and the average serpentine layer will thus contain relatively more ferrous Fe and be closer to berthierine.

A similar exercise for NREK7 indicates a formula of:

$$(Si_{3.14}Al_{0.87})(Al_{0.69}Fe^{3+}_{2.57}Fe^{2+}_{1.10}Mg_{0.42})O_{10}(OH)_8$$
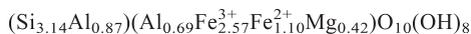
using a Mössbauer Fe ratio, and:

$$(Si_{3.08}Al_0.92)(Al_{0.60}Fe^{3+}_{3.30}Fe^{2+}_{0.19}Mg_{0.41})O_{10}(OH)_8$$

using the EELS Fe ratio which as itself would be close to odinite if no other ferric Fe-containing layers were present. Because we know ferric Fe-containing 2:1 layers exist, and the overall silica content is too small for odinite in the bulk chemical analysis, we conclude that the serpentine layers in these samples are berthierine-like, similar to that described by McCarty *et al.* (2004).

DISCUSSION

Because we were careful to collect only unweathered material, and many samples from the larger data set also contain siderite and pyrite, we consider it most unlikely that the Fe_2O_3 in the clay is a consequence of recent weathering. Even after wet-sieving, magnetic separation and drying, the peloids remained green with no trace of ferric Fe oxides. The EELS data confirm that Fe is only present in octahedral co-ordination, *i.e.* in clay minerals, and not in Fe oxides or hydroxides, while the Mössbauer and EELS data both indicate more Fe^{3+} than Fe^{2+}.

For the purpose of comparison with odinite we have selected the purest analysis of this mineral from the data in Bailey (1988). This is for a light green clay (sample 699) from the Los Islands in the Koukoure River mouth off Guinea. For comparison with berthierine we have selected the Jurassic (from Corby, UK) oolitic ironstone
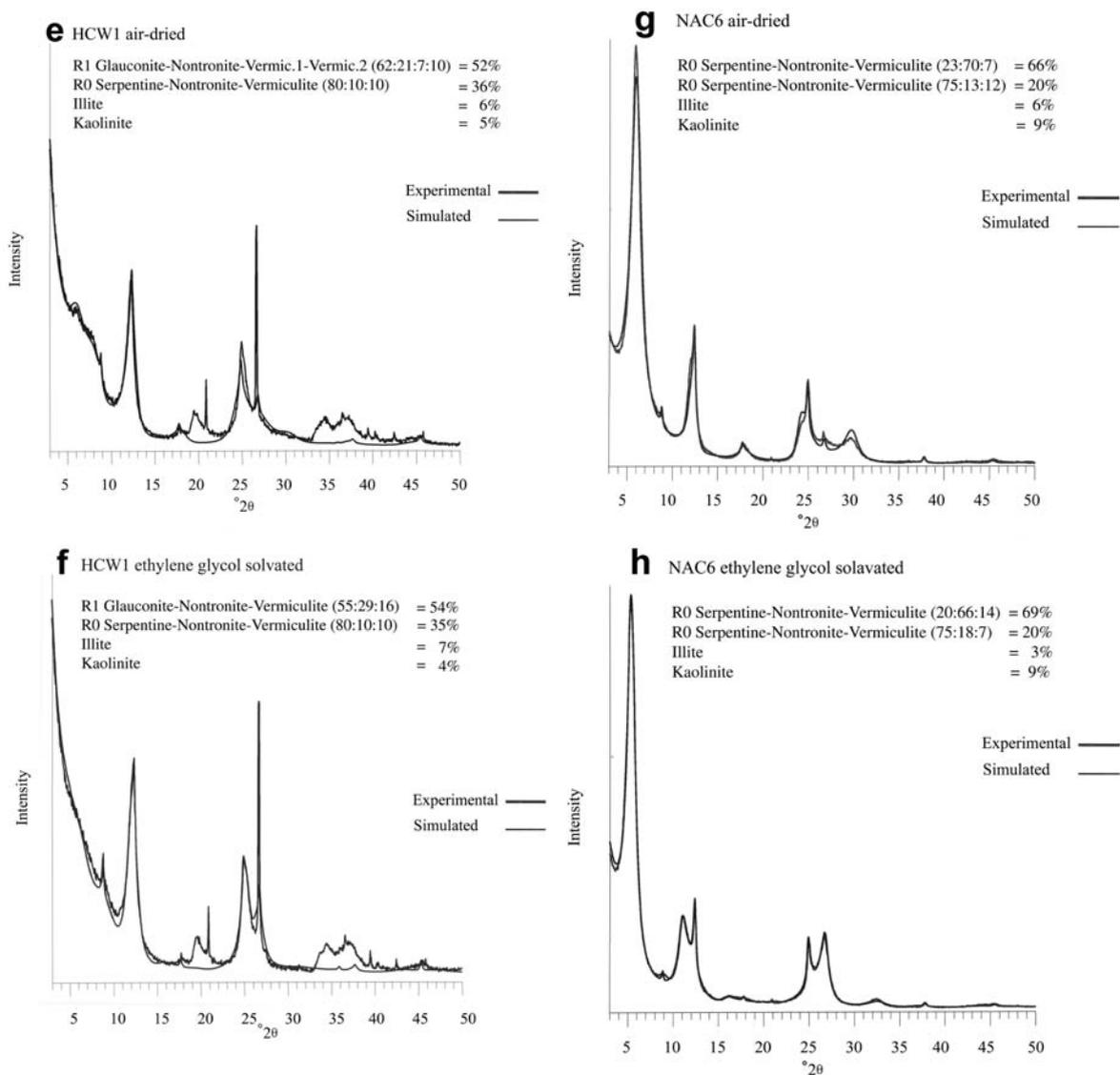
e HCW1 air-dried

R1 Glauconite-Nontronite-Vermic.1-Vermic.2 (62:21:7:10) = 52%
R0 Serpentine-Nontronite-Vermiculite (80:10:10)   = 36%
Illite   = 6%
Kaolinite   = 5%

Experimental ———
Simulated ———

g NAC6 air-dried

R0 Serpentine-Nontronite-Vermiculite (23:70:7) = 66%
R0 Serpentine-Nontronite-Vermiculite (75:13:12) = 20%
Illite   = 6%
Kaolinite   = 9%

Experimental ———
Simulated ———

f HCW1 ethylene glycol solvated

R1 Glauconite-Nontronite-Vermiculite (55:29:16) = 54%
R0 Serpentine-Nontronite-Vermiculite (80:10:10) = 35%
Illite   = 7%
Kaolinite   = 4%

Experimental ———
Simulated ———

h NAC6 ethylene glycol solavated

R0 Serpentine-Nontronite-Vermiculite (20:66:14) = 69%
R0 Serpentine-Nontronite-Vermiculite (75:18:7) = 20%
Illite   = 3%
Kaolinite   = 9%

Experimental ———
Simulated ———

Figure 7 (*contd.*)

analysis of Brindley and Youell (1953) because we believe that this clay and the Texas clay may have been deposited in similar shallow marine environments. In Table 4 the Nacogdoches and Hooker Creek data are normalized to 100% to facilitate comparison with published analyses for odinite and berthierine, keeping in mind that nontronite, Fe-vermiculite and glauconite layers are present in the Texas clay samples.

The Texas Fe-rich clay has a composition similar to berthierine in having significant ferrous Fe and having relatively small SiO_2. In addition, the Texas clay has a total Fe oxide wt.% considerably greater than that of odinite, and the proportion of MgO and the octahedral sheet charge are apparently intermediate between berthierine and odinite.

The Corby berthierine has <0.01 $Fe^{3+}/(Fe^{2+}+Fe^{3+})$, though values of up to 0.2 $Fe^{3+}/(Fe^{2+}+Fe^{3+})$ are known (Brindley, 1982). The odinite analysis from Bailey (1988) gives an $Fe^{3+}/(Fe^{2+}+Fe^{3+})$ of 0.75. We note that Odin (1988) obtained a value of 73.6% Fe^{3+} for the phyllite V (7 Å) component of verdine.

The chemical and X-ray analyses are consistent with an assemblage of mixed-layer clays containing berthierine-like layers, nontronite and vermiculite (Sp-N-V) and glauconite-nontronite-vermiculite (G-N-V) along with discrete illite and kaolinite, as indicated by XRD and FTIR. The sample NAC6 is different in that it contains two mixed-layer phases with different 7 Å layer contents. This sample also has a significant amount of ferrous Fe (Table 2). These mixed-layer assemblages are

Table 4. Comparison of normalized EDS data with published analyses for odinite (Bailey, 1988), berthierine (Brindley and Youell, 1953), nontronite (Goodman et al., 1976), Fe-smectite (Brigatti, 1983) and vermiculite (Newman, 1987). The weight % Fe values have been calculated using the $Fe^{3+}/(Fe^{2+}+Fe^{3})$ values determined by EELS because like the EELS analyses, these chemical data are for K^+- and Na^+-poor particles, inferred to be serpentine-rich. The % clay mineral layers were calculated from the air-dried simulation.

| Sample / Number of analyses	NREK1 $n=12$	std dev	NREK6 $n=7$	std dev	NREK7 $n=7$	std dev	HCW1 $n=5$	std dev	Odinite	Berthierine	Nontronite	Fe smectite	Vermiculite
% serpentine layers	not done		44.8		52.5		28.8						
% nontronite layers	not done		20.5		9.6		29.1						
% vermiculite layers	not done		6.0		9.4		8.8						
% illite and glauconite layers	not done		24.7		25.6		28.3						
% kaolinite layers	not done		4.0		3.0		5.0						
$Fe^{3+}/(Fe^{2+}+Fe^{3+})$	0.95		0.95		0.95		0.95		0.75	0.10	1?	1.00	0.92
SiO_2	38.22	1.20	33.68	1.40	32.39	1.92	41.44	1.43	42.51	26.65	47.65	62.20	45.10
Al_2O_3	15.47	0.97	13.45	4.30	13.61	1.31	18.41	1.20	14.41	25.88	0.74	16.99	14.15
Fe_2O_3	37.94	2.73	34.41	3.10	46.20	0.15	20.14	2.57	23.03	0.26	47.57	16.96	10.40
FeO	1.99	2.73	10.58	3.10	11.19	2.80	11.44	2.57	7.33	44.17	n.d.	—	0.90
TiO_2	0.20	0.06	0.14	0.01	0.01	0.09	0.18	0.18	0.47	—	—	0.13	0.06
MnO	0.07	0.08	0.07	0.01	0.07	0.08	0.17	0.16	0.39	—	—	0.08	0.19
MgO	5.38	0.07	6.34	0.02	2.89	0.08	5.78	0.10	11.45	3.05	0.32	2.65	23.81
CaO	0.06	0.30	0.09	0.20	0.99	0.60	0.70	0.75	—	—	—	—	5.36
Na_2O	0.11	0.06	0.19	0.02	0.19	0.07	0.25	0.06	tr.	—	3.73	0.16	—
K_2O	0.57	0.10	1.05	1.00	1.20	0.22	1.47	0.45	0.41	—	—	0.84	0.03
Totals	100.00		100.00		100.00		100.00		100.00	100.00	100.00	100.00	100.00

n.d. not determined
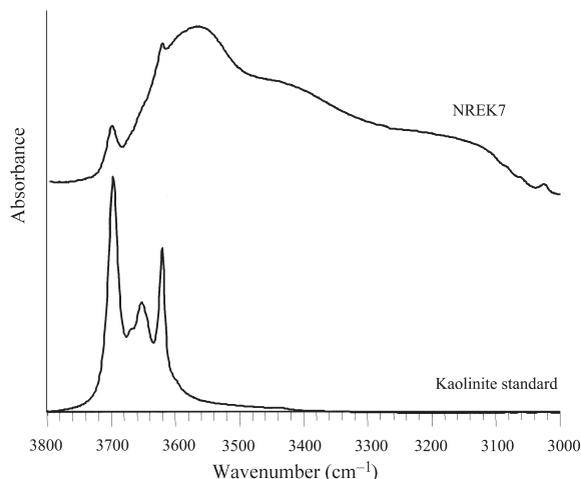
Figure 8. NREK7 and kaolinite standard FTIR plots.

similar to those described by McCarty *et al.* (2004) from the Isle of Wight Lower Greensand Formation. Given the range of % of each clay layer type in NREK6, NREK7 and HCW1, the analyses show a remarkably uniform chemical composition with low standard deviations (Table 4). The chemical composition of these three samples is also similar to that of NREK1, which has been shown by XRD to have no discrete 2:1 clay contamination of the Fe-rich 7 Å clay peloids. The principal inter-sample variation is in the relative proportions of wt.% Fe_2O_3 and SiO_2 (Table 4).

We infer from the observation that the soft brown peloids in the Claiborne Group are predominantly swelling clay, and that berthierine-like mixed-layer clays are only found in green, relatively indurated peloids. It appears that the brown swelling clay is being replaced by the green clay. The vermiculite layers in the Texas clay may indicate partial 'verdinization' of expandable 2:1 clay. A possible reaction is nontronite → vermiculite → berthierine-like phase. We know from results of XRD analyses of the matrix in which the peloids occur (to be published separately) that the peloids were almost certainly nontronite-rich at the time of deposition. Such a reaction would require dissolution of individual 2:1 layers in order to pre-cipitate 1:1 layers. It is not clear if the G-N-V is involved in the 'verdinization'. This too would require

dissolution of 2:1 layers (illite and smectite?). While the resulting mixed-layer clay phases are similar, either of these reactions would reflect a different mechanism to that proposed by McCarty *et al.* (2004) for the Cretaceous Lower Greensand Formation of southern England. McCarty *et al.* (2004) proposed a solid-state replacement of Al by Fe and Mg in both 2:1 and 1:1 layers, with illite replaced by glauconite, smectite by nontronite and kaolinite by berthierine where these layers exist in heterogeneous mixed-layer minerals. The mixed-layer clay reactions that McCarty *et al.* (2004) proposed are kaolinite-smectite-vermiculite → berthierine-nontronite-vermiculite; and illite-smectite-vermiculite → glauconite-nontronite-vermiculite. The two assemblages differ in that the Isle of Wight sediments were deposited in marginal environments with a bottom-water temperature of ~19ºC (Jones *et al.* 1994) while the Claiborne Group was deposited in a shallow marine environment with a bottom-water temperature of ~26ºC (extrapolated from data in Ivany *et al.* (2004). The Isle of Wight samples may have been deposited in a higher-energy environment. The differing pathways for Fe- and Mg-enrichment of clays may be controlled by microbiological processes, and hence, indirectly by the environment of formation.

Initially from the EELS data we thought that the serpentine layers had an odinite composition, which would have environmental implications. Odinite has not been reported in any form in sediments older than Miocene age and only from low-latitude sediments (Porrenga,1965; Odin, 1988). The detailed factors responsible for the preservation of these ferric 7 Å-rich mixed-layer clays are not well understood. Table 5 shows a compilation of latitude, facies and locality for published recent Fe-rich 7 Å clay occurrences. The identification of a berthierine-like clay in the Eocene from Texas, formed when Texas lay at a latitude of ~35ºN (Smith *et al.*, 1994), suggests that this clay can form outside the latitude range of recent odinite deposits (Table 5) and is consistent with the view that tropical conditions extended well beyond modern latitudinal limits (Ivany *et al.*, 2004). All published recent odinite occurrences indicate that it formed at a temperature ≥20ºC (Porrenga, 1965; Odin, 1988; Odin *et al.*, 1988a, 1988b; Odin and Sen Gupta, 1988), with a mean of 23.5ºC. Based on isotopic data for *Veneriacardia*, Ivany

Table 5. Compilation of published latitude, temperature, facies and locality data for recent occurrences of Fe-rich 7 Å clay.

Latitude	Locality	Facies	Reference
1ºN	Ogooue, Gabon	off river mouth	Odin (1988), Odin *et al.* (1988a)
0	Amazon	off river mouth	Rude and Aller (1989)
5ºN	Niger	delta front	Porrenga (1965)
11ºS	French Guiana	offshore	Odin *et al.* (1988b)
18ºN	India (E Coast)	offshore	Rao *et al.* (1995)
21ºS	New Caledonia	lagoonal	Odin (1988)

et al. (2004) calculated a surface seawater temperature for the Gulf Coast in the early Eocene of ~26ºC. Extrapolating from data in Zachos *et al* (1994) we get a temperature of 20ºC for the seawater in which the Texas clay formed. This is consistent with the surface temperature of Ivany *et al*. (2004) and Odin's observation (Odin, 1988) that temperature is a more fundamental control than latitude in the formation of authigenic serpentine layers. The question remains: were these Fe-rich 7 Å clay layers deposited as odinite with later Fe reduction by some, at present, unidentified process? Or were these 7 Å structures initially formed as berthierine-like layers? If the Fe-rich 7 Å clay was deposited, or formed at the time of deposition as odinite, could the Fe reduction be linked to loss of silica from tetrahedral sites as has been proposed for the low-temperature illitization of Fe-rich smectite (Huggett and Cuadros, 2006)?

CONCLUSIONS

Dark green clay pellets formed in a shallow-marine environment in the Claiborne Group of Texas consist of R0 serpentine-nontronite-vermiculite (Sp-N-V), R0 glauconite-nontronite-vermiculite (G-N-V), plus minor illite and kaolinite. The serpentine layers in the mixed-layer phases are berthierine-like. The Fe-rich mixed-layer clay responsible for the color is inferred to be the Sp-N-V. The 7 Å clay component of the mixed-layer clay was identified as berthierine-like on the basis of the $Fe^{3+}/(Fe^{2+}+Fe^{3+})$ which Mössbauer analysis indicates is ±0.70 for individual Fe-rich, K-poor clay particles. Thus, the 1:1 layers have more ferrous Fe than does odinite, especially when available ferric Fe is assigned to existing 2:1 layers in the mixed-layer assemblages. The vermiculite layers in the Texas clay may indicate partial 'verdinization' of expandable 2:1 clay. A possible reaction is smectite → vermiculite → berthierine-like serpentine layers. We estimate a temperature of 20ºC for the seawater in which the Texas clay formed. This is at the lower end of the range for modern occurrences of odinite.

ACKNOWLEDGMENTS

REFERENCES

Bailey, S.W. (1988) Odinite, a new dioctahedral-trioctahedral Fe^{3+}-rich 1:1 clay mineral. *Clay Minerals*, **23**, 237−248.

Bessons, G. Bookin, A.S., Dainyak, L.G., Rautureau, M., Tsipursky, S.I., Tchoubar, C. and Drits, V.A. (1983) Use of diffraction and Mössbauer methods for the structural and crystallochemical characterisation of nontronites. *Journal of Applied Crystallography* **16**, 374−383.

Bhattacharyya, D.P. (1983) Origin of berthierine in ironstones. *Clays and Clay Minerals*, **31**, 173−182.

Brigatti, M.F. (1983) Relationships between composition and structure in Fe-rich smectites. *Clay Minerals*, **18**, 177−186.

Brindley, G.W. (1951) The crystal structures of some chamosite minerals. *Mineralogical Magazine*, **29**, 502−525.

Brindley, G.W. (1982) Chemical compositions of berthierines − a review. *Clays and Clay Minerals*, **30**, 153−155.

Brindley, G.W. and Youell, R.F. (1953) Ferrous chamosite and ferric chamosite. *Mineralogical Magazine*, **30**, 57−70.

Burst, J.F. (1958) "Glauconite" ooids: their mineral nature and applications to stratigraphic interpretations. *American Association of Petroleum Geologists Bulletin*, **42**, 310−327.

Calvert, C.C., Brydson, R., Banks, D.A. and Lloyd, G.E. (2001) Quantification of Fe-oxidation state in mixed valence minerals: a geochemical application of EELS. *Institute of Physics conference Series Number 168*: Section 6, 251−254.

Calvert, C.C., Brown, A.P. and Brydson, R. (2005) Determination of the local chemistry of iron in inorganic and organic materials. *Journal of Electron Spectroscopy and Related Phenomena*, **143**, 173−187.

Chamley, H. (1989) *Clay Sedimentology.* Springer Verlag, Berlin, 623 pp.

Drits, V.A. and Tchoubar, C. (1990*) X-ray Diffraction by Disordered Lamellar Structures*. Springer-Verlag, Berlin, 371 pp.

Drits, V.A., Lindgreen, H. and Salyn, A. (1997) Determination by X-ray diffraction of content and distribution of fixed ammonium in illite-smectite. Application to North Sea illite-smectites. *American Mineralogist*, **82**, 79−87.

Drits, V.A., Lindgreen, H., Sakharov, B.A., Jakobsen, H.J., Salyn, A. and Dainyak, L.G. (2002) Tobelitization of smectite during oil generation in oil-source shales. Application to North Sea illite-tobelite-smectite-vermiculite. *Clays and Clay Minerals*, **50**, 82−98.

Goodman, B.A., Russell, J.D., Fraser, A.R. and Woodhams, F.W.D. (1976) A Mössbauer and infrared spectroscopy study of the structure of nontronite. *Clays and Clay Minerals*, **24**, 53−59.

Huggett, J.M. and Cuadros, J. (2006) Low temperature illitization of smectite in the Late Eocene and Early Oligocene of the Isle of Wight (Hampshire basin), UK. *American Mineralogist* (in press).

Imam, M.B. and Shaw, H.F. (1985) The diagenesis of Neogene clastic sediments from the Bengal Basin, Bangladesh. *Journal of Sedimentary Petrology*, **55**, 665−671.

Ivany, L.C., Wilkinson, B.H., Lohmann, K.C., Johnson, E.R., McElroy, B.J. and Cohen, G.J. (2004) Intra-annual isotopic variation in Venericardia bivalves: implications for early Eocene temperature seasonality, and salinity on the U.S. Gulf Coast. *Journal of Sedimentary Petrology*, **74**, 7−19.

Jackson, M.L. (1985) *Soil Chemical Analysis − Advanced Course*, 2nd edition, 11th printing. Published by the author, Madison, Wisconsin, USA.

Jones, C.E., Jenkyns, H.C., Coe, A.L. and Hesselbo, S.P. (1994) Strontium isotopic variations in Jurassic and Cretaceous seawater. *Geochimica et Cosmochimica Acta*, **58**, 3061−3074.

MacEwan, D.M.C. and Wilson, M.J. (1980) Interlayer and intercalation complexes of clay minerals. Pp. 197−248 in: *Crystal Structures of Clay Minerals and their X-ray Identification* (G.W. Brindley and G. Brown, editors*).* Monograph **5**, Mineralogical Society, London.

Macquaker, J.H.S., Taylor, K.G., Young, T.P. and Curtis, C.D. (1996) Sedimentological and geochemical controls on ooidal ironstone and 'bone-bed' formation and some comments on their sequence stratigraphic significance. Pp.

97−107 in: *Sequence Stratigraphy in British Geology* (S. Hesselbo and D.N. Parkinson, editors). Special Publication **103**, Geological Society, London.

McCarty, D.K. and Reynolds, R.C. Jr. (1995) Rotationally disordered illite-smectite in Paleozoic K-bentonites. *Clays and Clay Minerals*, **43**, 271−284.

McCarty, D.K., Drits, V.A., Sakharov, B., Zvyagina, B.B., Ruffell, A. and Wach, G. (2004) Heterogeneous mixed-layer clays from the Cretaceous Greensand, Isle of Wight, southern England. *Clays and Clay Minerals*, **52**, 552−575.

Moore, D.M. and Reynolds, R.C. (1997*) X-ray diffraction and the Identification and Analysis of Clay Minerals*, 2nd edition. Oxford University Press, New York, 378 pp.

Newman, A.C.D. (1987) *Chemistry of Clays*. Monograph **6**, Mineralogical Society, London 480 pp.

Odin, G.S. (1988) The verdine facies from the lagoon off New Caledonia. Pp. 57−81 in: *Green Marine Clays* (G.S. Odin, editor). Developments in Sedimentology, **45**. Elsevier, Amsterdam.

Odin, G. S. and Sen Gupta, B.K. (1988) The geological significance of the verdine facies. Pp. 205−247 in: *Green Marine Clays* (G.S. Odin, editor). Developments in Sedimentology, **45**. Elsevier, Amsterdam.

Odin, G.S., Debenay, J.P. and Masse, J.P. (1988a) The verdine facies deposits identified in 1988. Pp. 131−157 in: *Green Marine Clays* (G.S. Odin, editor). Developments in Sedimentology, **45**. Elsevier, Amsterdam.

Odin, G.S., Mackinnon, I.D.R. and Pujos, M. (1988b) The verdine facies off French Guyana. Pp. 105−130 in: *Green Marine Clays* (G.S. Odin, editor). Developments in Sedimentology, **45**. Elsevier, Amsterdam.

Plançon, A. (2004) Consistent modeling of the XRD patterns of mixed-layer phyllosilicates. *Clays and Clay Minerals*, **52**, 47−54.

Porrenga, D.H. (1965) Chamosite in Recent sediments of the Niger and Orinoco delta. *Geologie Mijnbouw*, **44**, 400−403.

Porrenga, D.H. (1967) Glauconite and chamosite as depth indicators in the marine environment. *Marine Geology*, **5**, 495−501.

Rao, V.P. Thamban, M. and Lamboy, M. (1995) Verdine and glaucony facies from surficial sediments of the eastern continental margin of India. *Marine Geology*, **127**, 105−113.

Rude, P.D. and Aller, R.C. (1989) Early diagenetic alteration of lateritic particle coatings in Amazon continental shelf sediment. *Journal of Sedimentary Petrology*, **59**, 704−716.

Ryan, P.C. and Hillier, S. (2002) Berthierine/chamosite, corrensite and discrete chlorite from evolved verdine and evaporite associated facies in the Jurassic Sundance Formation, Wyoming. *American Mineralogist*, **87**, 1607−1615.

Sakharov, B.A., Lindgreen, H., Salyn, A.L. and Drits, V.A. (1999) Determination of illite-smectite structures using multispecimen XRD profile fitting. *Clays and Clay Minerals*, **47**, 555−566.

Shterenberg, L.E., Stepanova, K.A., Stravinskaya, E.A. and Uranova, O.V. (1968) Composition and origin of micro-concretions of the profundal zone of Lake Punnis-Harvi. *Lithology and Mineral Resources*, **3**, 733−738.

Smith, A.G., Smith, D.G. and Funnell, B.M. (1994) *Atlas of Mesozoic and Cenozoic Coastlines.* Cambridge University Press, Cambridge, UK, 99 pp.

Taylor, K.G. (1990) Berthierine from the non-marine Wealden (Early Cretaceous) sediments of south-east England. *Clay Minerals*, **25**, 391−399.

Taylor, K.G. (1998) Spatial and temporal variations in early diagenetic organic matter oxidation pathways in Lower Jurassic mudstones of eastern England. *Chemical Geology*, **145**, 47−60.

Van Houten, F.B. and Purucker, M.E. (1984) Glauconitic ooids and chamositic ooids, favorable factors, constraints, and problems. *Earth Science Reviews*, **20**, 211−243.

Vincent, F.S. and Ewing, T.E. (2000) Lower Claiborne Regional Stratigraphic Architecture, Southeast Texas to East Central Louisiana Gulf Coasts. *Association of Geological Societies Transactions*, **50**, 759−760.

Wermund, E.G. (1961) Glauconite in early Tertiary sediments of Gulf Coast Province. *Bulletin of the American Association of Petroleum Geologists*, **45**, 1667−1696.

Yancey, T.E. and Davidoff, A.J. (1994) Paleogene sequence stratigraphy of the Brazos River Section, Texas. *Gulf Coast Association of Geological Societies Field Trip Guide*, 112 pp.

Zachos, J.C. (1993) Occurrence of the Spatangid echinoid Maretia Arguta (Clark) in the Middle Eocene Texas. *Journal of Paleontology*, **67**, 148−150.

Zachos, J.C., Stott, L.D. and Lohmann, K.C. (1994) Evolution of early Cenozoic marine temperatures. *Paleoceanography*, **9**, 353−387.